

VĚDECKÉ SPISY VYSOKÉHO UČENÍ TECHNICKÉHO V BRNĚ

*Edice PhD Thesis, sv. 872*

*ISSN 1213-4198*

*thesis*  
**IS**

*Ing. František Ondreáš*

**Thermomechanical Response  
of Polymer Nanocomposites  
with Preparation Protocol  
Controlled Nanoparticle Dispersion**



**CENTRAL EUROPEAN INSTITUTE OF TECHNOLOGY BUT**

**STŘEDOEVROPSKÝ TECHNOLOGICKÝ INSTITUT VUT**

**THERMOMECHANICAL RESPONSE OF POLYMER  
NANOCOMPOSITES WITH PREPARATION PROTOCOL  
CONTROLLED NANOPARTICLE DISPERSION**

TERMOMECHANICKÉ CHOVÁNÍ POLYMERNÍCH NANOKOMPOZITŮ  
S DISPERZÍ NANOČÁSTIC KONTROLOVANOU POMOCÍ  
PŘÍPRAVNÉHO PROTOKOLU

ZKRÁCENÁ VERZE PH.D. THESIS

<b>OBOR</b>	<b>Pokročilé materiály</b>
<b>AUTOR PRÁCE</b>	<b>Ing. František Ondreáš</b>
<b>ŠKOLITEL</b>	<b>prof. RNDr. Josef Jančář, CSc.</b>
<b>OPONENTI</b>	<b>prof. Ing. Ivan Chodák, DrSc. RNDr. Libor Matějka, DSc.</b>
<b>DATUM OBHAJOBY</b>	<b>11. prosince 2018</b>

Brno 2019

**Keywords:**

Polymer nanocomposites, nanoparticle self-assembly, relaxation properties, mechanical properties

**Klíčová slova:**

Polymerní nanokompozity, samouspořádávání nanočástic, relaxační vlastnosti, mechanické vlastnosti

**MÍSTO ULOŽENÍ PRÁCE**

Originál dizertační práce je uložen na Studijním oddělení Středoevropského technologického institutu Vysokého učení technického v Brně.

**DECLARATION**

I declare that this thesis has been composed solely by myself under the supervision of prof. RNDr. Josef Jančář, CSc. and that all quotations of the literary sources are accurate and complete. The presented results are the property of Central European Institute of Technology at Brno University of Technology and all commercial uses are allowed only if approved by both the supervisor and the director of the Central European Institute, BUT. The thesis includes copyrighted content which further use may require a permission from the copyright owner.

© František Ondreáš, 2019

ISBN 978-80-214-5725-6

ISSN 1213-4198

## Table of Contents

1. Theoretical part.....	5
1.1 Nanoparticle organization in a polymer matrix .....	5
1.2 Properties of polymer nanocomposites .....	5
2. Experimental part.....	6
3. Results and discussion.....	9
3.1 Controlling nanoparticle spatial organization in polymer matrix .....	9
3.2 Relaxation properties .....	13
3.3 Mechanical properties of polymer nanocomposites .....	17
3.4 Correlation between relaxation and mechanical properties .....	20
4. Conclusions .....	22
5. References .....	25
6. Author's CV .....	29
7. Abstract .....	31



# 1. Theoretical part

As reported many times<sup>1-3</sup>, polymer nanocomposites can provide properties unachievable by traditional composites. Rigorous investigation of common natural materials<sup>1, 3-7</sup> have shown that nature can create materials with advanced properties, for example simultaneous high stiffness and toughness or combined functionality and tailored mechanical properties. Nature can control self-assembly process to create hierarchical structures where original building blocks – molecules or nanoparticles, are assembled into structures that are again used as building blocks during creating more complex structure on larger scales. Current experimental approaches are meeting only challenge of preparation of simple nanocomposite systems.

## 1.1 Nanoparticle organization in a polymer matrix

A key to full utilization of the potential of polymer nanocomposites (PNCs) lies in the ability to control spatial organization of nanoparticles (NPs) in polymer matrix over multiple length scales. Despite the large volume of literature published on control of NP dispersion in polymer matrices<sup>8-41</sup>, no generally accepted model quantitatively describing all the aspects of NP organization in polymer liquids has been proposed. The state of NP spatial organization critically affects the PNC properties. Since any given property requires a specific NP organization, no single length scale NP spatial organization can optimize all macroscopic properties simultaneously.

Nanoparticles can self-assemble into three limiting structures in polymer liquids. They can be organized into contact aggregates, chain bound clusters, or can be individually dispersed in polymer matrix. Particles in aggregates interact directly with each other by weak interparticle Van der Waals forces. Therefore, the whole aggregate seems like one big fragile particle. This reduces specific surface area that determines nanocomposite properties such as relaxation and mechanical response. Therefore, polymer nanocomposites with aggregates are undesirable. In the case of dispersion of individual nanoparticles in polymer matrix, maximum surface area can interact with surrounding chains and specific surface area equals to effective interface area. This is ideal state for a fundamental study, because interface area, on which interactions occur, is known, and also maximal possible amount of modified matrix is achieved in such system. Polymer nanocomposites with good dispersion of nanoparticles are characterized by significantly enhanced mechanical properties<sup>8, 9, 42</sup>. In the case of clusters, particles don't interact directly with each other, but through chains between them. Clusters can be considered independent entities dispersed in a polymer matrix. Thereby hierarchical system with two levels is formed.

## 1.2 Properties of polymer nanocomposites

Addition of nanoparticles with large specific surface area to polymer matrix leads to amplification of a number of molecular processes resulting from interactions between nanofiller surface and polymer chains. It results in significant changes of relaxation and mechanical response. Ability of nanoparticles to assemble into extended structures can bring extraordinary effects. Properties of polymer nanocomposites cannot be described by the common micromechanics models. Therefore, it is necessary to develop new approach to describe this class of materials connecting discrete nano scale molecular dynamics and micro scale continuum mechanics<sup>8</sup>.

A three phase model considering nanoparticles, bulk matrix also “interface modified matrix” was developed<sup>8, 43-46</sup>. Volume and properties of the surface modified matrix depend on the specific interface area (i.e. filler loading and dispersion state) and strength of interactions, which are determined by chemical composition of polymer chains and functional groups on the surface of particles. Another variable not considered so far is the rigidity of the polymer chain. NP–polymer system with attractive interactions can form immobilized layer of chains around NPs with different molecular packing and dynamics from original matrix. The nanoparticle with the repulsive interactions can form layer of chains with enhanced mobility and chain packing differing from the bulk matrix. These assumptions suggest that besides particles and matrix, immobilized segment layer and frustrated packing layer exist in polymer nanocomposites.

Immobilization/repulsion of polymer segments and presence of frustrated polymer layer is reflected upon relaxation properties by changing molecular packing and dynamics. Influence of the nanoparticles on macroscopic properties is more significant near the glass transition, where interactions between polymer segments and nanoparticles surface have greater impact on polymer dynamics than on segments with “frozen” dynamics deeply in glassy state. Vitrification occurs when relaxation time of molecular motions responsible for rearrangement of characteristic segments become longer than the experimental time frame. Local segmental motion freezes during the glass transition without any significant change of the structure of the glass forming liquid. Significant impact of nanoparticles on glass transition temperature was reported in literature<sup>8, 12, 17, 23, 29, 44, 47-50</sup>. The reason for nanoparticles altering vitrification is the immobilization/repulsion of polymer segments by nanoparticles. Different changes of glass transition temperature reported<sup>47</sup> for similar systems are caused by insufficient knowledge of all parameters influencing dynamics and molecular packing of polymer nanocomposites investigated.

Jancar et al.<sup>51, 52</sup> compared mechanical properties of microparticle (MP) and NP filled poly(methyl methacrylate) (PMMA). It was found that MP-sized filler with small specific interface area did not disturb segmental packing and mobility in a significant volume of the matrix. Effect of MPs on the elastic modulus, yield stresses, and strain hardening modulus was described by a simple volume replacement models. However, NPs modified the packing and dynamics on the segmental scale with behavior indescribable by any classical continuum model. Varying NP influence on mechanical properties was found at different temperatures and thermal histories supporting the theory of immobilization as the segmental scale reinforcing mechanism. Kinetic analysis of both upper and lower yields, and strain hardening modulus showed that activation energies increase with larger specific interface area. The results revealed that attractive SiO<sub>2</sub>–PMMA interactions increased the energy required to activate the segmental rearrangements associated with plastic flow and strain hardening.

## 2. Experimental part

PMMA with lower number average molecular weight,  $M_n$ , PC, and PS were of commercial grade – Plexiglas 8N, Makrolon 2407C, and Krasten 154, respectively. PMMA with greater  $M_n$ , and both PVAc were purchased from Sigma Aldrich. Glassy matrices were chosen in order to avoid influence of crystallization on the spatial organization of nanoparticles<sup>53, 54</sup> and the final properties<sup>53-56</sup>. Spherical nanoparticles were used to avoid effects of additional structural variables such as aspect ratio and orientation. Colloidal bare silica nanoparticles dispersed in isopropanol with particle diameter of  $20 \pm 4$  nm was supplied by Nissan Chemicals under commercial name IPA-ST. Pyrolytic nanosilica from Sigma Aldrich with primary particles with diameter of 7 nm was also used. Additionally, zinc oxide nanoparticles

doped with 2 wt. % aluminium oxide nanoparticles (AZO) with diameter of approximately 15 nm were purchased from US Research Nanomaterials. Magnetite nanoparticles also from US Research Nanomaterials with diameter of approximately 15-20 nm were also used.

Nanofillers were ultrasonicated in a solvent employing an ultrasonic tip (Bandelin Sonopuls, SRN). Firstly, resonance frequency was found and then ultrasonication was performed. Ultrasonication was divided into  $t_{on}$  of 0.1 s and  $t_{off}$  of 2.5 s time intervals with overall time of 5 minutes. Subsequently, solution of nanoparticles was added to a polymer solution with concentration of 66.7 mg of a polymer per one milliliter of a solvent (about 5.3 vol. %) which corresponds to semi-dilute region. Nanoparticle loading of final composites was 0.1, 0.5, 1, 2.5, 5, 7.5, and 10 vol. %. Various solvents were used: acetone, acetone-toluene 1:1 mixture (volumetric ratio), toluene, ethyl acetate, tetrahydrofurane, and dichlormethane. Dissolved PNCs were rigorously mixed at 1200 RPM using a magnetic stirrer for 1 hour. Then, PNC mixture was cast onto a flat sheet, dried at 140 °C for PMMA, 150 °C for PC and PS, and 80 °C for PVAc for 12 hours at atmospheric pressure. Dried PNCs were mechanically grinded using IKA A11 basic analytic mill (IKA, GE). Powdered PNCs were dried for 6 days in a vacuum oven to ensure removal of solvent residues. Drying efficiency was checked utilizing thermogravimetric analysis. Dried samples were compression molded at 190 °C for PMMA and PS, 260 °C for PC, and 80 °C for PVAc and at 300 kN into 1 and/or 0.5 mm thick sheets by means of the LabEcon 300 Press. (Fontijne, NL). The samples were cooled down under pressure to the laboratory temperature at a cooling rate of approximately 30 K·min<sup>-1</sup>. Specimens with the desired geometry were cut from these sheets.

Morphology of the PNCs was determined by means of the transmission electron microscopy (TEM) and ultra-small-angle X-ray scattering (USAXS). TEM (FEI, CZ) provides a direct view of silica spatial arrangement in polymer matrix. Ultratomed slides of PNCs with constant thickness of approximately 50 nm were prepared (Leica Microsystems, GE). TEM observations were performed using Morgagni 268D 100 kV transmission electron microscope (FEI, CZ), STEM MIRA3 (TESCAN, CZ) and STEM Verios 460L (FEI, CZ). TEM snapshots were analyzed with the help of image analysis software – size of elements and interparticle distances were determined. USAXS provides the average shape and internal structure information of nanoparticles arrangement in the polymer matrix. USAXS was performed using X-ray diffractometer Smartlab (Rigaku, JPN) with copper rotating anode, 2 × 220 germanium monochromator and 2 × 220 germanium USAXS analyzer. USAXS patterns were analyzed by means of the Guinier and Porod laws.

Oscillatory shear small deformation tests and dynamic mechanical analysis (DMA) were carried out to provide thermomechanical properties of prepared polymer nanocomposites. Shear test corresponding to low deformation levels (0.5 %) were performed in the dynamic mode under the strain controlled conditions with the plate-plate geometry employing ARES G2 rheometer (TA Instruments, USA). Thermal environment equipped with an air oven ensures a temperature control within 0.1 °C. Weak axial force was used in order to gently compensate gap position with respect to thermal expansion and retraction occurred during a test. Frequency sweeps from 0.01 to 20 Hz in a temperature ramp 10 °C were performed for the temperature ranging from 200 to 150 °C. Dynamic mechanical analysis was carried out using DMA RSA G2 (TA Instruments, USA). Measurements were performed in linear viscoelastic regime at deformation amplitude of 0.05 %, and frequency of 1 Hz. DMA analysis was used to characterize relaxation behavior in the transition regime and to determine glass transition temperature.

Mechanical properties were measured utilizing Zwick Roell Z010 (Zwick-Roel, CH). Mechanical measurements were conducted using dog-bone shaped specimens in tension and cylindrical specimens were utilized for compression tests at true strain – true stress conditions. The experiments were carried for strain rates ranging from  $10^{-5}$  to  $10^{-1} \text{ s}^{-1}$  at various temperatures. Long-term tensile creep measurements were performed at  $80 \text{ }^{\circ}\text{C}$  and various constant loading.

### 3. Results and discussion

#### 3.1 Controlling nanoparticle spatial organization in polymer matrix

The control of NP spatial organization in polymer matrix is a prerequisite for transforming PNCs from scientifically interesting materials to technologically viable engineering materials. By varying the solvent strength, different nanoparticle (NP) organizations were prepared in the model PMMA/colloidal SiO<sub>2</sub> PNC. Mixture of individually dispersed NPs and contact aggregates were identified for tetrahydrofuran (THF) (Figure 1), individually dispersed NPs for acetone and ethyl acetate (Figure 2 and 3), chain bound clusters for acetone–toluene 1:1 mixture (Figure 4), and contact aggregates for toluene (Figure 5), respectively.

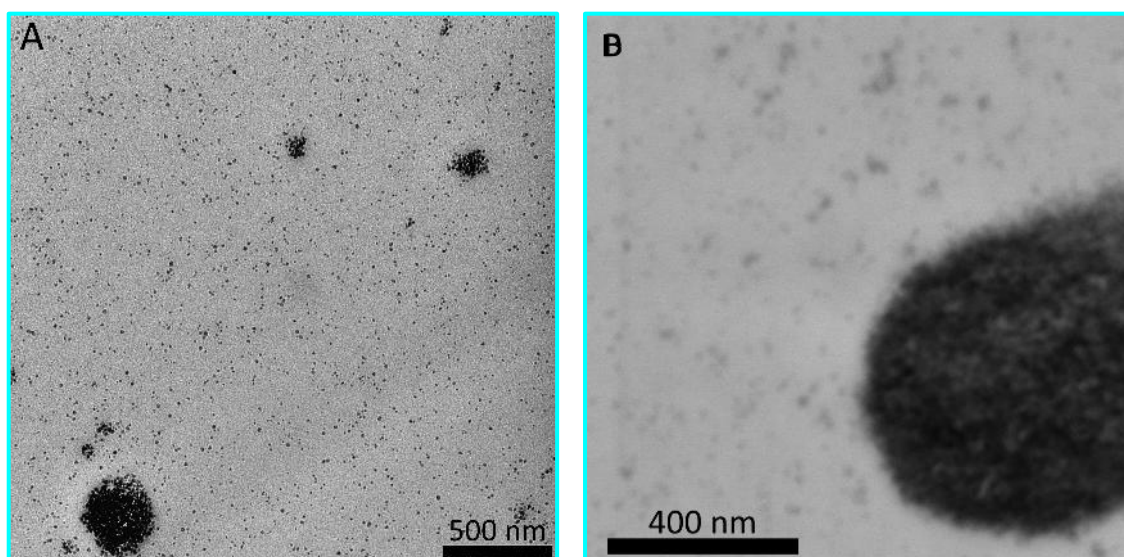


Figure 1: TEM images of THF series 50 kg/mol PMMA/colloidal SiO<sub>2</sub> PNC with loadings 1, and 5 vol. % for A, and B, respectively.

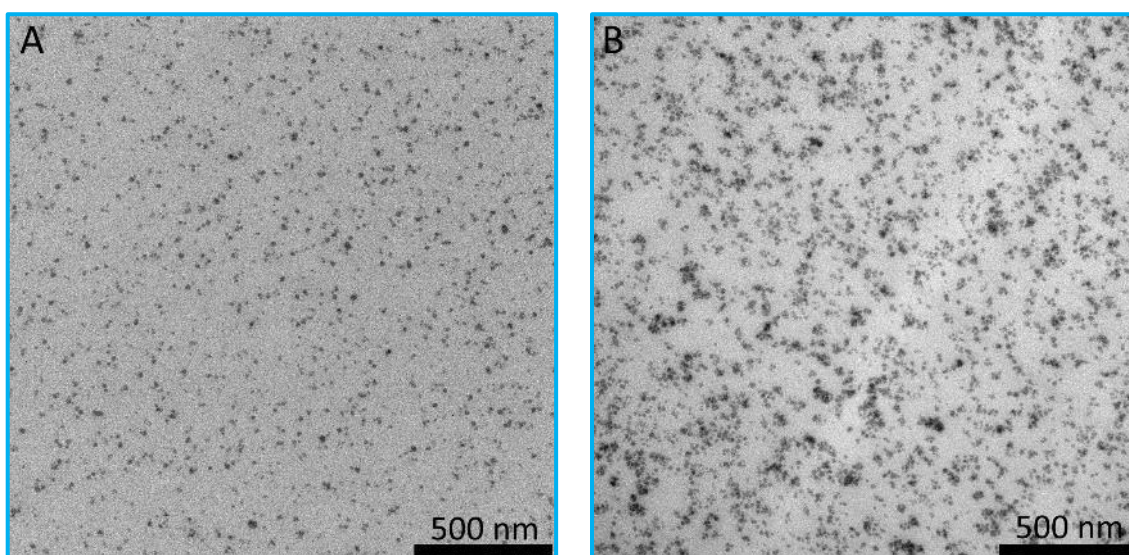


Figure 2: TEM images of acetone series PMMA/colloidal SiO<sub>2</sub> PNC with loadings 1, and 5 vol. % for A, and B, respectively.

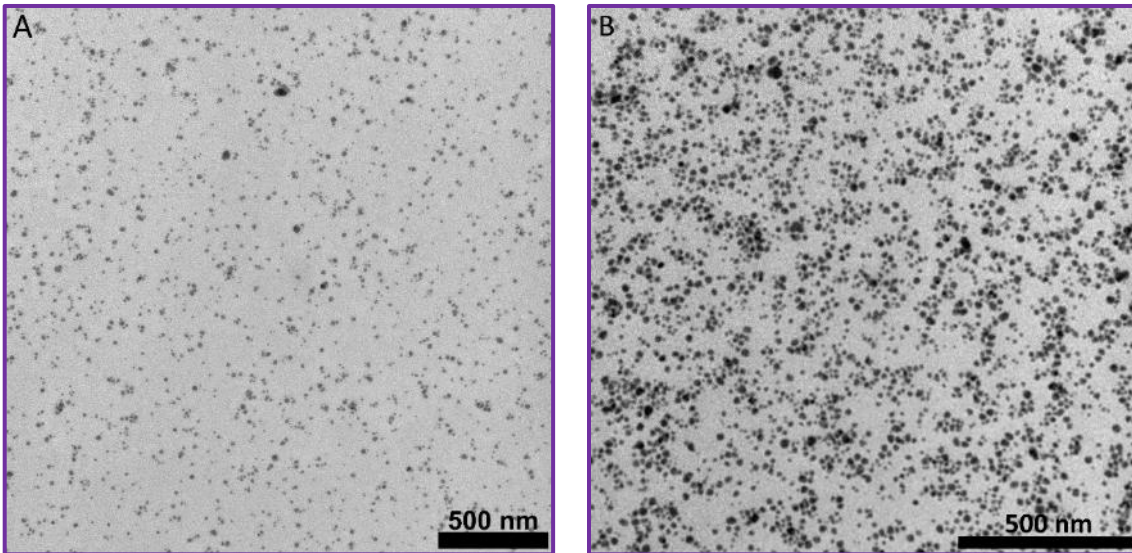


Figure 3: TEM images of ethyl acetate series PMMA/colloidal SiO<sub>2</sub> PNC with loadings of 1 and 5 vol. % for A, and B, respectively.

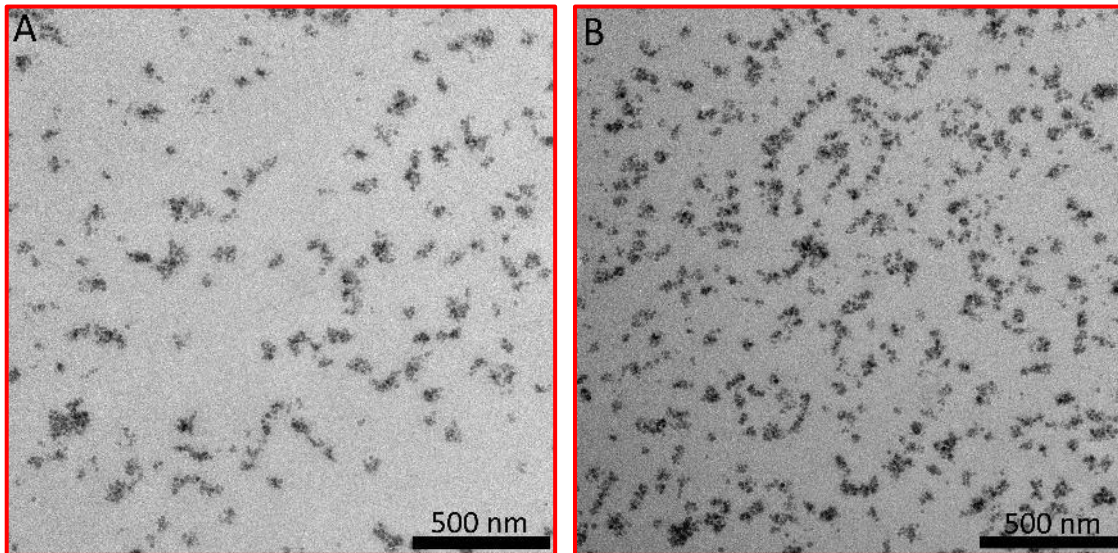


Figure 4: TEM images of acetone-toluene 1:1 mixture series PMMA/colloidal SiO<sub>2</sub> PNC with loadings 1, and 5 vol. % for A, and B, respectively.

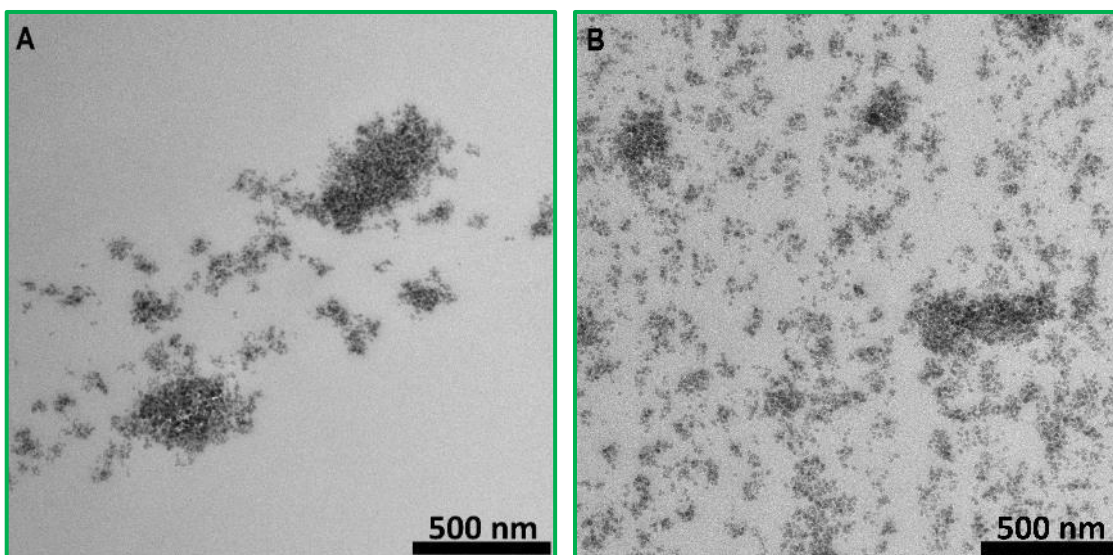


Figure 5: TEM images of toluene series PMMA/colloidal SiO<sub>2</sub> PNC with loadings 1, and 5 vol. % for A, and B, respectively.

The interparticle distance in the PMMA/1 vol. % colloidal SiO<sub>2</sub> prepared from acetone and ethyl acetate was determined using image analysis to be approximately 33 and 40 nm, respectively. The results showed that the dispersion of isolated NPs in the PNCs prepared from acetone is only achieved at low filler loadings up to 1 vol. % (Figure 2A) while above 5 vol.%, silica NPs tend to aggregate (Figure 2B). It is probably a consequence of shortened interparticle distance which promoted the short range Van der Waals interaction always acting against good dispersion. The aggregate size was relatively small (about 26–34 nm) and grew gradually with filler content. Dispersion of individual NPs in PNCs prepared from ethyl acetate were also attained only below 1 vol. % (Figure 3A). In the ethyl acetate prepared PNCs, the TEM micrographs suggest (Figure 3B), that NPs began to form clusters with diameter of approximately 32 nm, above 1 vol. %.

Chain bound clusters (Figure 4) were formed in the PMMA using the 1:1 acetone-toluene solvent mixture. Three populations of cluster sizes were found with few individually dispersed NPs. The smallest clusters contained 2 to 3 NPs (the least frequent occurrence), the intermediate clusters contained 5 to 9 NPs, and the large clusters consisted of 16 to 26 particles (the most frequent occurrence). Theoretical models<sup>57</sup> suggest gradual increase of cluster size with time assuming that individual particles form small clusters consisting of two to three nanoparticles and once formed, these elementary clusters connect building up larger clusters. Clusters were observed in all samples of acetone-toluene series and the cluster size of approximately 43 nm was preserved throughout the whole concentration range investigated.

Finally, preparing the PNC utilizing THF (Figure 1) or toluene (Figure 5) resulted in the presence of contact NP aggregates with the average size of approximately 400 and 500 nm, respectively. However, aggregates in THF and toluene PNCs have different origin. Aggregates in PNCs prepared from THF are formed due to depletion attraction arising from high affinity between silica NPs and THF molecules. Aggregates in PNCs prepared from toluene have their origin in low interaction strength between toluene and silica NPs leading to separation of NPs. Mixture of individually dispersed NPs and contact aggregates was found for all NP volume fractions investigated in PNCs prepared from THF as shown in Figure 1. Both populations of aggregates presented in PNCs of toluene series grew with increasing silica content.

Clusters and aggregates were treated as the elementary structural units where applicable for the purpose of TEM image analysis. Interelement distance was determined from image analysis. A fair agreement between the experimental results and theoretical study of random distribution of monodisperse spheres<sup>58, 59</sup> was found.

Taking into consideration experimental results discussed above, we propose a general approach to analyze structural variables affecting stable NP dispersion in glass forming polymer liquids. For silica NPs in the PMMA solution, the interfacial interactions are dominated by the acid–base interactions between acidic silanol groups on the silica surface and the basic groups of the PMMA and the solvent<sup>60–64</sup>. Interaction enthalpies were calculated using Drago’s formula from the E and C constants reported in the literature<sup>64, 65</sup>. Values for the toluene were taken as a mean average of benzene and xylene, since the data for toluene was not available. This uncertainty has no significant effect on the interpretation of experimental data due to the close E and C values for benzene and xylene, both being significantly smaller than the E and C for acetone. The E and C for the 1:1 acetone-toluene mixture were obtained by averaging the values for acetone and toluene.

The calculated donor–acceptor interaction enthalpies of for prepared model PNCs are shown in the Figure 6A. The highest value of the negative interaction enthalpy,  $-\Delta H = 8.9 \text{ kcal}\cdot\text{mol}^{-1}$ , in this study is found between the THF and silanol groups on the silica surface, which is significantly stronger than the attraction between PMMA and silica ( $-\Delta H = 4.0 \text{ kcal}\cdot\text{mol}^{-1}$ ). In combination with the large excess of solvent in the mixture, it suggests that the adsorption onto silica is dominated by the THF molecules and a strong solvation shell is formed around NPs, which, in turn, repels the polymer chains from the vicinity of NPs and causes NP aggregation due to depletion attraction.

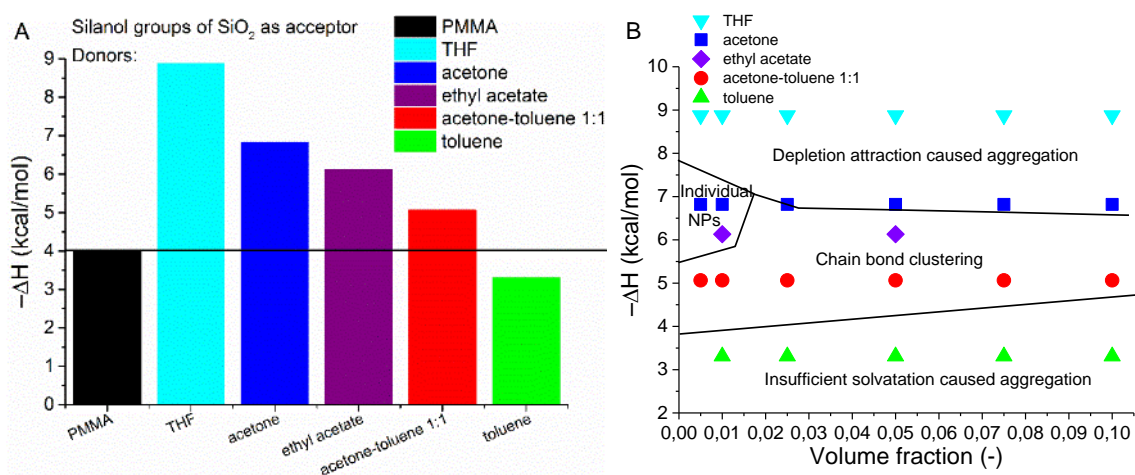


Figure 6: (A) Bar diagram of donor-acceptor enthalpies of adducts of silanol groups of SiO<sub>2</sub> nanoparticles with PMMA and various solvents. (B) Volume fraction dependence of silica–solvent interaction enthalpy phase diagram of PMMA/SiO<sub>2</sub> PNCs.

The interaction enthalpies of silica-acetone ( $-\Delta H = 6.8 \text{ kcal}\cdot\text{mol}^{-1}$ ) and ethyl-acetate-silica ( $-\Delta H = 6.1 \text{ kcal}\cdot\text{mol}^{-1}$ ) are smaller than the THF-silica, but still stronger than that of the silica-PMMA couple. Since the solvent molecules are favorably adsorbed onto silica, the stabilization of the experimentally observed dispersion of individual NPs is likely caused by the solvation effect in addition to the previously suggested<sup>15</sup> repulsion of adsorbed polymer layer induced by polymer-NP attraction. Unlike in the previous studies using extremely slow solvent removal<sup>15</sup>, the dispersion of isolated NPs obtained in our experiments is maintained through relatively fast solvent removal upon the PNC solidification. Viscosity of the liquid

PNC progressively increases significantly slowing down the NP diffusion and, thus, reducing their ability to aggregate. This explains the previously reported experimental results<sup>11</sup> claiming that the fast solvent evaporation often leads to improved NP dispersion. The strength of attraction between the 1:1 acetone-toluene mixture and silica ( $-\Delta H = 5.1 \text{ kcal}\cdot\text{mol}^{-1}$ ) prevented the contact aggregation. However, it was not sufficient to stabilize the dispersion of individual NPs. Since the PMMA-silica attraction is only slightly weaker than that between silica and mixed solvent, the PMMA chains may locally replace the solvent and adsorb onto the NP surface. This competition between the polymer and solvent adsorption is proposed as the mechanism by which the chain bound NP clusters are formed. The low enthalpy of attraction between toluene and silica ( $-\Delta H = 3.3 \text{ kcal}\cdot\text{mol}^{-1}$ ) is reflected by the inability of the solvent to stabilize the dispersed NPs leading to contact aggregation. The strength of attraction between PMMA and silica ( $-\Delta H = 4.0 \text{ kcal}\cdot\text{mol}^{-1}$ ) is greater than that for the toluene-silica interaction, which suggests that polymer adsorption onto the NP surface takes place as a competitive process to contact aggregation, as manifested by the presence of two populations of NP ensembles.

The dependence of the NP-solvent acid-base interaction enthalpy on the filler volume fraction was used to construct phase diagram of the PMMA/SiO<sub>2</sub> PNCs investigated (Figure 6B). Only a narrow window was found of conditions suitable for spatial organization of individually dispersed NPs for the medium strong NP-solvent attraction enthalpy at relatively low NP volume content ( $\approx 1 \text{ vol. } \%$ ). Strengthening the NPs-solvent attraction led to aggregation caused by the depletion attraction. Slight lowering of the interaction enthalpy led to chain bound clusters in the entire range of the filler volume fractions investigated. Further decrease of the interaction enthalpy led to aggregation caused by insufficient solvation of NPs by the solvent.

### 3.2 Relaxation properties

Glass transition temperature can be used as a probe to investigate molecular mobility changes. The dependence of the difference between the glass transition temperature of PNCs and the neat PMMA,  $\Delta T_g$ , on volume fraction for various dispersion states is shown in Figure 7A. Increase of  $T_g$  was found for all the PNCs investigated. Attractive PMMA-SiO<sub>2</sub> interactions were expected due to the hydrogen bonding between ester groups of PMMA and surface silanol groups of silica<sup>66</sup>. The greatest increase of  $T_g$  was recorded for PNCs with individually dispersed NPs. The NP content dependence of  $\Delta T_g$  exhibits an initial rapid increase compared to the neat PMMA followed by a weak growth at higher concentrations which suggests that the dynamics of almost all polymer chains was already frustrated at the loading as low as 0.5 vol. %. The additional increase of  $\Delta T_g$  would then be caused by the increasing volume of the immobilized segmental layers onto NP surface. Hamieh et.al<sup>67</sup> found that  $T_g$  increase for syndiotactic PMMA induced by silica equals approximately to 5 °C, which supports the hypothesis suggested. Clustered system showed a gradual rise of  $T_g$  with increasing NP volume fraction. The lowest  $\Delta T_g$  was found in PNCs with aggregated. The results fall onto one curve when related to the specific interface area (Figure 7B) or reciprocal value of interelement distance (Figure 7C). NP organization independent increase of  $T_g$  with the surface of elements in PNC and the reciprocal value of interelement distance suggests slower dynamics in vicinity of NPs caused by immobilization. Apparently, these two structural variables are more appropriate for interpretation of  $T_g$  changes than the volume fraction alone. This approach could shed more light onto the discrepancy found in literature dealing with the volume fraction dependence of  $T_g$  of PNCs<sup>8, 26, 47, 48</sup>.

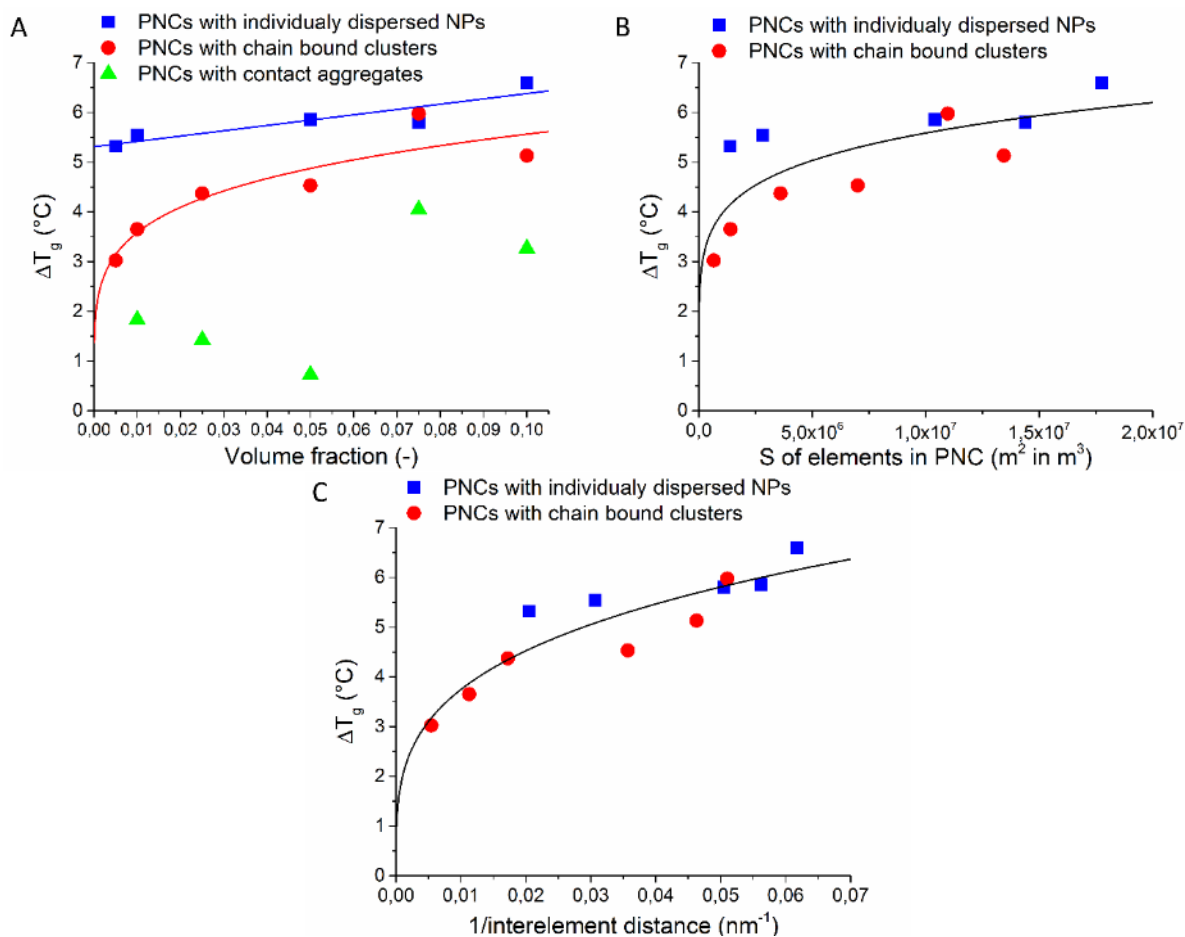


Figure 7: dependence of  $\Delta T_g$  on (A) volume fraction, (B) surface area of elements in PNC, and (C) reciprocal value of interelement distance of various PNCs.

The melt rheology of a glassy polymer in the range of its typical processing temperature is greatly altered by the presence of NPs determining the PNC processability and practical applicability and brings the rheological evaluation into the light of interest with practical consequences. The dependence of reptation time on the filler volume fraction showed differences between various nanostructures (Figure 8A). However, the reptation time of various nanostructures fell onto one curve when plotted against interface area (Figure 8B). The obtained increase of reptation time has not only origin in the increase in the primitive path contour length, but also because chains must reptate through several domains of slower dynamics near the surface of the NPs. These experimental results are in good agreement with molecular modeling reports<sup>68</sup>. The internal structure of clusters was neglected in the calculation of the interfacial surface and they were treated as compact entities. Since the data collapsed onto the same curve as the dispersion of individual NPs, it seems that the bridged chains inside the clusters were unable to contribute significantly to the determined macroscopic response within the investigated volume fraction, temperature and frequency range.

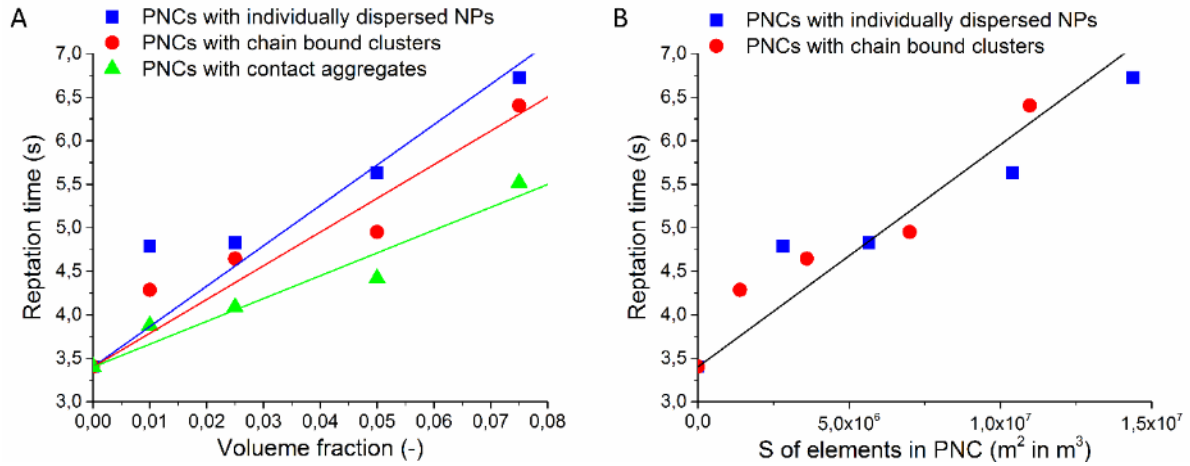


Figure 8: Dependence of reptation time at 190 °C on (A) volume fraction and (B) effective surface area of elements in PNC.

Chain dynamics of the rubbery plateau was retarded by the attractive NP-polymer interaction. Immobilized segments reached relaxation times similar to glassy segments while unaffected bulk dynamics exhibited unchanged dynamics with several orders magnitude longer relaxation times<sup>8, 69-71</sup>. The existing volume replacement continuum mechanics models<sup>72-74</sup> for the composition dependence of the plateau modulus were not able to describe the dependence of the relative modulus on the NP volume fraction (Figure 9A). An additional segmental scale reinforcing mechanism characterized by the composite modulus reduced to the matrix modulus and appropriate continuum micromechanics model were proposed to be directly related to the interfacial area<sup>75</sup>. An important structural difference arisen when this reinforcing mechanism was related to the total interfacial area (Figure 9B). Plateau modulus of individually dispersed NPs tend to slightly decrease or stagnate with the increasing interfacial surface (volume fraction) up to about  $5 \cdot 10^6 \text{ m}^2/\text{m}^3$  (2.5 vol. %), where it becomes overwhelmed by a rapid growth. Clusters exhibited modulus stagnation up to  $3 \cdot 10^6 \text{ m}^2/\text{m}^3$  (2.5 vol. %) followed by gradual modulus increase which was more pronounced than the corresponding dispersion of individual NPs. As suggested by the simulation of Long, et al.<sup>76, 77</sup>, the strong increase might be caused by the percolation of the immobilized domains around the NPs due to the weakly worsening dispersion state and filler morphology. This overpowered dependence on the interfacial surface lead to a conclusion that NPs assembled into close-packed clusters experience a significant contribution of the internal structure to macroscopic properties originating from the highly affected bridging chains inside the clusters and also from the inter-cluster percolation at higher volume fractions. Plateau moduli of the PNCs were reduced to the Guth-Smallwood model<sup>72-74</sup> and matrix moduli were calculated by Equation 5:

$$G_{0\text{matrix}}^N = \frac{G_{0c}^N}{G_{G-S}} = \frac{G_{0c}^N}{1+2.5v_f+14.1v_f^2}, \quad (1)$$

where  $G_{0\text{matrix}}^N$  is matrix plateau modulus,  $G_{0c}^N$  nanocomposite plateau modulus,  $G_{G-S}$  modulus calculated by the Guth–Smallwood model, and  $v_f$  volume fraction. Modified matrix moduli were used for calculation of the number of entanglements per one chain in the PNCs (Equation 1). Dependence of the number of NP induced entanglements per one chain on the volume fraction is shown in Figure 9C. The number of entanglements per one chain increased in all PNCs investigated suggesting that NPs act as entanglements attractors. The greatest increase was found in clustered PNCs and the lowest in aggregated PNCs.

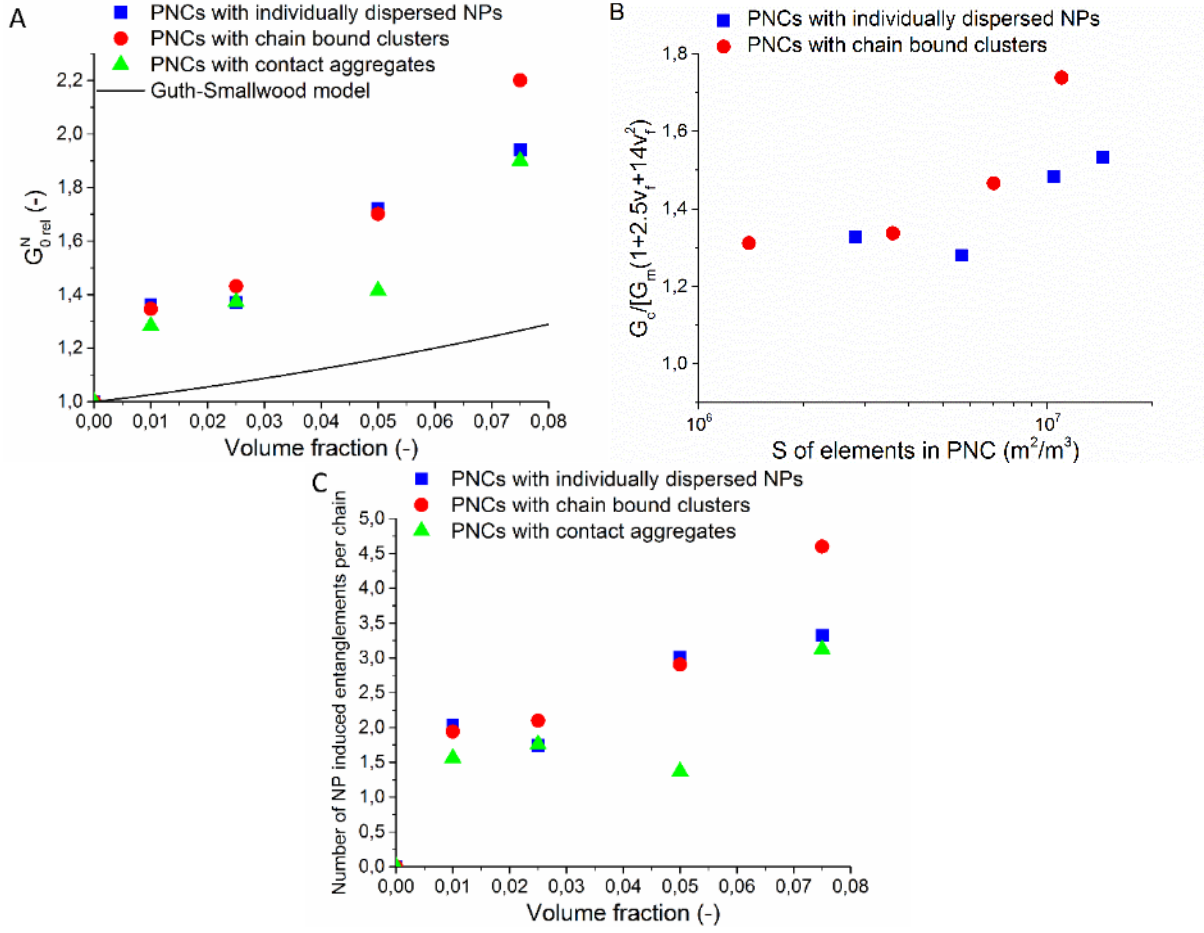


Figure 9: Dependence of plateau modulus on (A) volume fraction, (B) plateau composite modulus reduced to the matrix modulus and appropriate continuum micromechanics model on surface of elements in PNC, and (C) dependence of number of entanglements per one chain on volume fraction of PNCs with various NP spatial organization.

Dependence of the relative zero shear rate viscosity on the filler volume fraction is also shown in Figure 10. For the purpose of further analysis, PNCs investigated are assumed to be suspensions of particles in a high-viscosity continuum of polymer segments. Under this assumption, dependence of the relative zero shear rate viscosity on the filler volume fraction can be described by the Equation 2<sup>21, 78-81</sup>:

$$\eta_{r0} = 1 + 2.5k\phi + P\phi, \quad (2)$$

where  $\eta_{r0}$  is relative zero shear rate viscosity, 2.5 is Einstein coefficient,  $k$  is the parameter that characterizes influence of polymer adsorption on intrinsic viscosity<sup>21, 78-81</sup>, and  $P$  is the particle interaction coefficient that characterizes effect of particle interactions on the suspension viscosity<sup>21, 78-81</sup>.

Adsorption of polymer segments onto surface of particles increases their hydrodynamic size. This effect is more pronounced with decreasing particle size. Therefore, significant discrepancy characterized by the  $k$  parameter was found from Einstein coefficient of 2.5 derived for non-interacting particles. The highest  $k$  value (15) exhibited PNCs with individually dispersed NPs due to the highest effective interface area. The  $k$  value (11) of PNCs with chain bound clusters was close to the value of PNCs with individually dispersed NPs. The lowest  $k$  (5) value was found for PNCs with contact aggregates, but their  $k$  value

still differed significantly from the Einstein coefficient. This effect was ascribed to the adsorption of polymer segments onto smaller aggregates that have still relatively large surface area. Adsorbed polymer layer thickness was calculated by means of Equation 3:

$$h = \sqrt[3]{\frac{3Vk}{4\pi}} - r, \quad (3)$$

where  $h$  is the thickness of the affected polymer layer,  $V$  is the element volume,  $k$  is the above mentioned parameter, and  $r$  is the element radius. Radii determined by image analysis of TEM snapshots were used (average radius of 15 nm for series of individually dispersed NPs and 20 nm for series with chain bound clusters). The thickness of affected polymer layer of  $23 \pm 1$  nm was approximately the same for the various NPs spatial organizations. The obtained affected layer thickness suggests that every NP influences dynamics of approximately 2 coils in the direction perpendicular to the NP surface. It means that chain dynamics of all polymer chains is affected by NPs below the interparticle distance of approximately 40 nm. It corresponds to about 1 vol. % filler loading for individually dispersed NPs and 5 vol. % for chain bound NP clusters. The PNCs with chain bound clusters had the highest particle interaction coefficient (497) due to strong adsorbed chains mediated interactions of particles in closely packed clusters. The lowest  $P$  value was found for PNCs with individually dispersed NPs (21) because of their largest interelement distances and absence of clusters. PNCs with aggregated NPs exhibited intermediate  $P$  value (139).

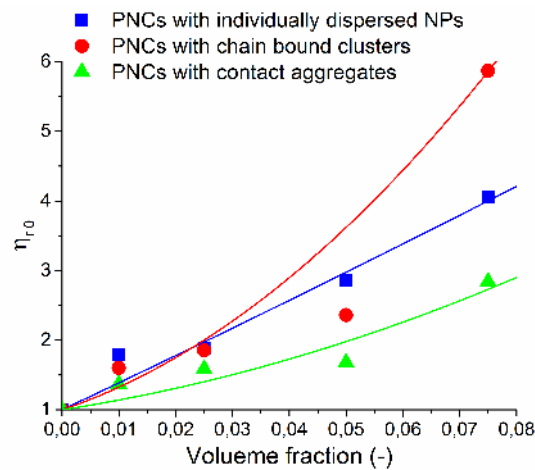


Figure 10: Dependence of zero shear rate viscosity on volume fraction fitted with Cross model.

### 3.3 Mechanical properties of polymer nanocomposites

Significant enhancement of elastic modulus was found near the glass transition. In the glassy state, relaxation time difference between the affected and bulk chains is not as pronounced as in the rubbery state<sup>8</sup>, but the affected chains could exhibit a different path through the vitrification process during cooling, resulting in a different position on the energy landscape<sup>82</sup>. The dependence of the elastic modulus behaved similarly to the above discussed plateau modulus. The existing volume replacement continuum mechanics models<sup>83-85</sup> for the composition dependence of the elastic modulus were not able to describe the dependence of the relative modulus on the NP volume fraction (Figure 11A). An additional segmental scale reinforcing mechanism characterized by the composite modulus reduced to the matrix modulus and appropriate continuum micromechanics model were proposed to be directly

related to the interfacial area<sup>75</sup>. An important structural difference was found when this reinforcing mechanism was related to the total interfacial area (Figure 11B). The initial increase of the elastic modulus at low concentrations was much more pronounced for individually dispersed NPs compared to chain bound clusters. The elastic modulus of individually dispersed NPs tend to slightly decrease or stagnate with the increasing interfacial surface (volume fraction) up to about  $10^7 \text{ m}^2/\text{m}^3$  (5 vol. %), where it becomes overpowered by a rapid growth. Clusters exhibited modulus stagnation up to  $3 \cdot 10^6 \text{ m}^2/\text{m}^3$  (2.5 vol. %) followed by gradual modulus increase. As suggested by the simulation of Long, et al.<sup>76, 77</sup>, the strong increase might be caused by the percolation of the immobilized domains around the NPs due to the weakly worsening dispersion state and filler morphology. This overwhelmed dependence on the interfacial surface lead to a conclusion that NPs assembled into close-packed clusters experience a significant contribution of the internal structure to macroscopic properties originating from the highly affected bridging chains inside the clusters and also from the inter-cluster percolation at higher volume fractions.

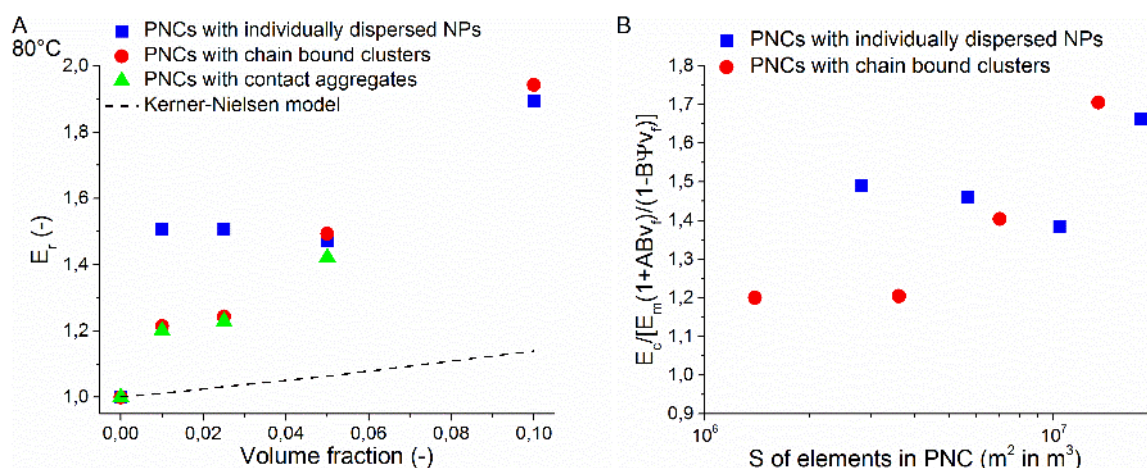


Figure 11: Dependence of relative elastic modulus on (A) volume fraction and (B) plateau composite modulus reduced to the matrix modulus and appropriate continuum micromechanics model on surface of elements in PNC with various NP spatial organization measured in tension at temperature of 80 °C and strain rate of  $10^{-2} \text{ s}^{-1}$ .

Considering a different deformation of the polymer chains in bulk matrix, in the vicinity of NPs, and in the inner structure of clusters, PNCs can exhibit a complex macroscopic response consisting of these contributions. Mechanical properties of PMMA/SiO<sub>2</sub>, exhibiting the three different nanostructures were investigated (Figure 12A). All samples showed ductile deformation response at 80 °C. The crossover between  $\alpha$  and  $\alpha + \beta$  regime remained localized near the strain rate of  $10^{-3} \text{ s}^{-1}$ . PNCs with individual NPs exhibited the most pronounced increase of the yield stress, aggregates the lowest, and clusters lied between them. Moreover, slopes of yield stress-strain rate dependence and related activation volumes did not change compared to the neat PMMA. Quite different situation was found at 60°C, Figure 12B. While the neat PMMA was macroscopically brittle, it still followed the ductile yielding regime whereas embrittlement of PNCs with aggregates was so extensive that they did not follow ductile yielding regime. PNCs with clusters followed ductile yielding with different slope of yield stress–strain rate dependence compared to the neat PMMA. Moreover, the response was macroscopically ductile at certain strain rates, possibly due to the hierarchical nature of clusters. Clusters can represent structured inclusions yielding hierarchical composite endowing both intrinsic and extrinsic deformation processes to become active.

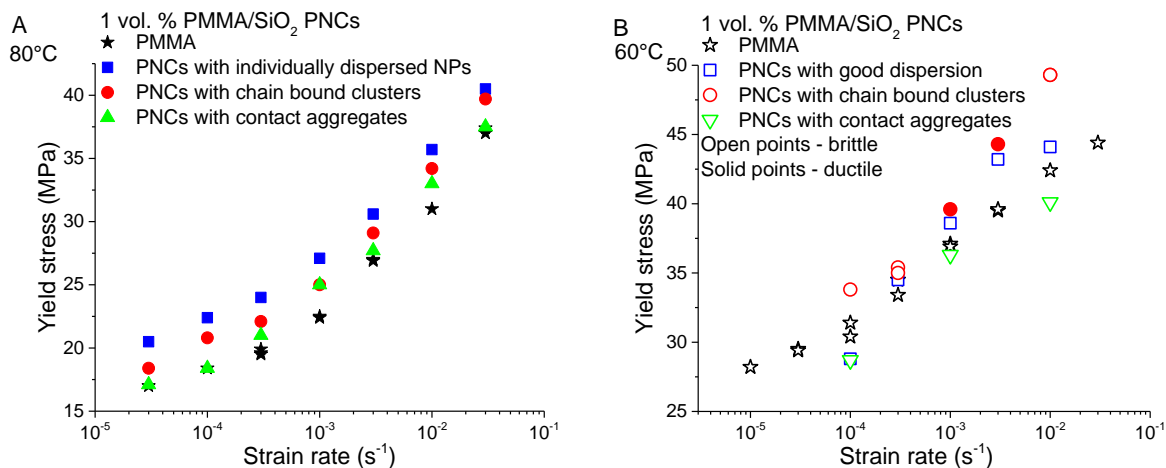


Figure 12: Strain rate dependence of yield stress of PNCs with various NP spatial organization measured in tension at (A) 80 and (B) 60 °C.

The nanocomposite yield stress was found to increase compared to the neat matrix in all PNCs investigated with the only exception of 5 vol. % PNC with contact aggregates which supports the presence of attractive interactions in nanosilica–PMMA assumed earlier (Figure 13). The strongest enhancement of the yield stress was found for PNCs with individually dispersed NPs due to the highest effective surface area. Yield stress stagnation between 1 and 5 vol. % of NPs can be explained by gradual aggregation – a decrease of the effective surface area as suggested by Dorigato et.al<sup>86</sup>. However, similar situation was found for a clustered system, where no aggregation was observed. A possible explanation could be a saturation – majority of chains are influenced by NPs even at low filler volume fraction; therefore, no further increase of the yield stress was found. Quite different behavior was found for PNCs with contact aggregates. Dependence of the yield stress on the filler volume fraction of PNCs with contact aggregates can be fitted with the Pukanszky model up to 2.5 vol. % with interaction parameter  $B = 8$ . Further increase of volume fraction led to a sharp decrease of the yield stress. Extensive aggregation caused the presence of critical defects; therefore 5 vol. % PNC with contact aggregates had macroscopically brittle response and its yield stress fitted well to the modified Nicolais–Narkis model.

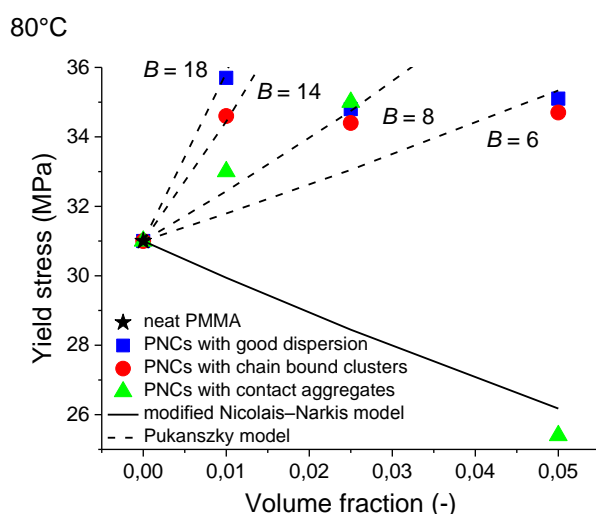


Figure 13: Dependence of yield stress on volume fraction of PNCs with various NP spatial organizations at 80°C and strain rate of  $10^{-2} \text{ s}^{-1}$ . Solid line shows the modified Nicolais Narkis

model<sup>87, 88</sup>. Dash lines shows the Pukanszky model<sup>87</sup> with various values of interaction parameter  $B$ .

Good durability performance is a critical parameter of a high-end material design. Long-term mechanical response was investigated on various nanocomposites<sup>89-92</sup>; nevertheless, the fundamental effect of the NP organization has still been missing. Therefore, long-term creep behavior of 1 vol. % PNCs were compared with neat PMMA matrix, Figure 14. Different long-term response was found for different NP spatial organizations. PNCs with individually dispersed NPs showed a shift of more than one order of magnitude to longer failure times with the same slope of the dependence as for the neat PMMA, while PNCs with clusters and aggregates were shifted to shorter times and steeper slope suggesting a different mechanism of the long-term response for different NP spatial organizations.

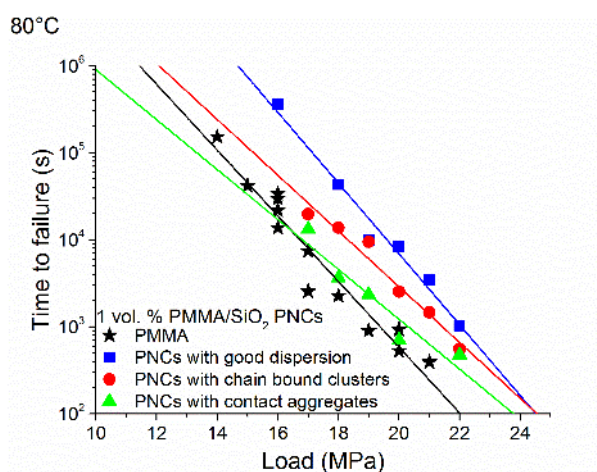


Figure 14: Dependence of time to failure on load of neat PMMA matrix and PNCs with various NP spatial organizations measured in tensile creep at 80 °C.

### 3.4 Correlation between relaxation and mechanical properties

The enhancement of the yield stress by NPs introduced into the polymer matrix was reported in previous chapters (Figure 15A). The yield stress was reduced to the distance from the glass transition temperature ( $T_g - T$ ) to further investigate this phenomenon (Figure 15B). It was found that the strain rate dependence of the reduced yield stress of the neat PMMA matrix and PNCs converged into a single curve. It suggests that the distance from the glass transition distance controls the investigated yield behavior. Chains were further from its  $T_g$  in PNC than in PMMA matrix, occupying a different location in energy landscape, when measured at a single temperature. NPs significantly altered the packing and dynamics of the surrounding chains compared to the bulk. A similar effect of NPs on the glass transition temperature and yield stress showed that the dynamics responsible for the vitrification process is crucial also in the yielding phenomenon operating at the same length and time scale.

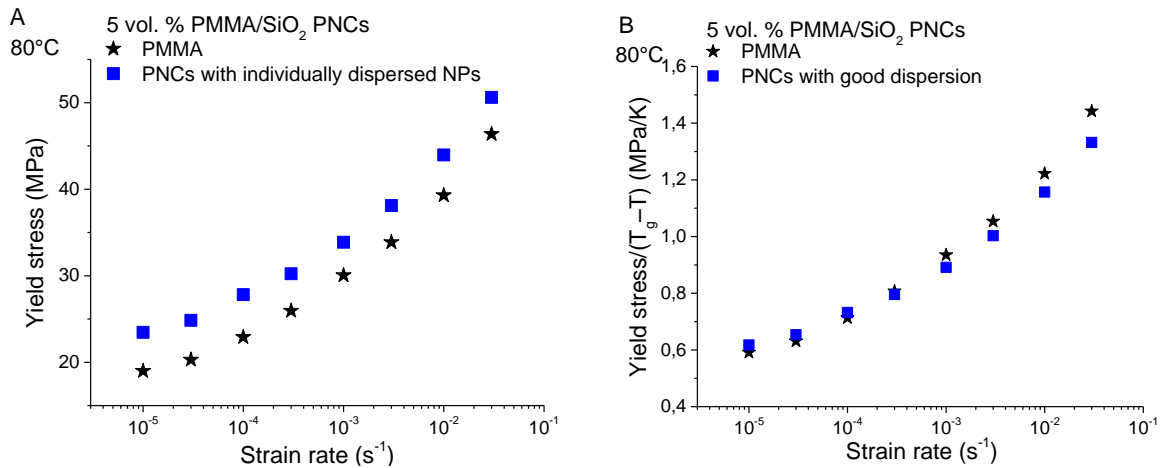
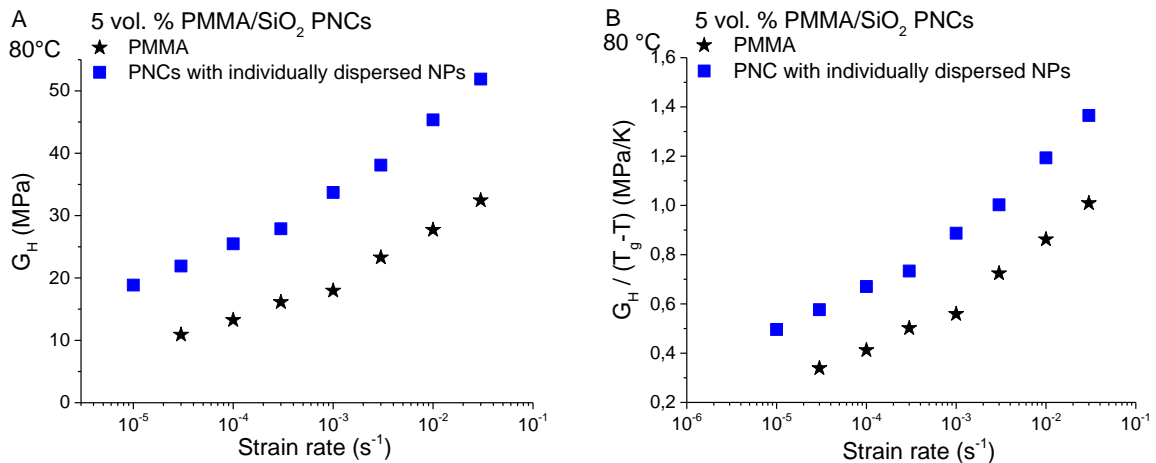


Figure 15: Dependence of (A) yield stress and (B) yield stress reduced to distance from glass transition temperature on strain rate of PMMA matrix and 5 vol. % PMMA/SiO<sub>2</sub> PNCs with individually dispersed NPs measured in compression at 80 °C.

The pronounced increase of the strain hardening modulus of PNCs with individually dispersed NPs compared to the neat PMMA matrix was also reported in previous chapters (Figure 16A). Strain hardening modulus was reduced to the distance from the glass transition ( $T_g - T$ ) similarly as in the previous case, but no convergence of the PNC and the matrix strain rate dependence was found (Figure 16B). It means that the dynamics at strain hardening regime is not similar with the local segmental dynamics responsible for glass transition. The strain hardening modulus was also reduced to the number of entanglements per one chain (Figure 16C) which caused the PNC and the neat matrix data converged into a single curve. NPs act as entanglements attractors altering the polymer dynamics in plateau region. The results suggests that the dynamics responsible for the strain hardening response lies in the same time and length scale as the dynamics in the plateau region.



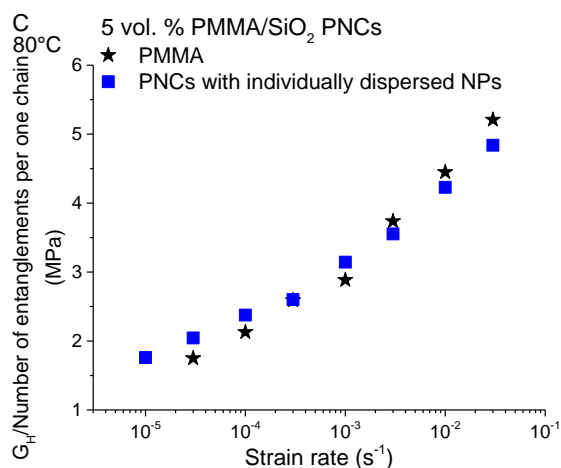


Figure 16: Dependence of (A) strain hardening modulus, (B) strain hardening modulus reduced to distance from glass transition, and (C) strain hardening modulus reduced to number of entanglements per one chain on strain rate of neat PMMA matrix and 5 vol. % PMMA/SiO<sub>2</sub> PNCs with individually dispersed NPs measured in compression at 80 °C.

## 4. Conclusions

Nanostructure control, relaxation and mechanical properties of nanocomposites with polymer glass matrix and ceramic nanoparticles were investigated. A deep investigation was performed on PMMA/SiO<sub>2</sub> model system and subsequently broadened to systems with another matrices and NPs to generalize the obtained results. First, a method enabling to control the NPs spatial organization was devised. Subsequently, properties of polymer nanocomposites with governed dispersion state were investigated. Relaxational and mechanical properties of PNCs with precisely determined nanostructure were determined to provide valuable data characterizing this promising class of materials. Furthermore, NPs were utilized as probes that affect molecular packing and dynamics of polymer chains. The determined relaxational and mechanical properties were linked to provide information about the molecular processes behind deformation response of polymer glasses and their nanocomposites.

Polymer nanocomposites with controlled NP dispersion state were prepared by solution blending technique with fast solvent evaporation. Individually dispersed NPs, chain bound clusters, contact aggregates and mixture of individually dispersed NPs and contact aggregates were identified by TEM and USAXS techniques. Solvent-particle interactions were suggested as the dominant structure governing factor among the complex interplay of particle-polymer-solvent interactions at investigated conditions. The solvent-particle interaction strength was quantified by Drago's donor-acceptor interaction enthalpy<sup>60-65</sup>. Matrix and solvent had basic character and particle surface functional groups had acidic character. Influence of NP volume fraction on NP dispersion was also investigated. Worsening of dispersion state of individually dispersed NPs was found with increasing volume fraction of NPs due to shortening of the interparticle distance – increase of the particle-particle attractive interaction strength. Phase diagram of acid-base interaction enthalpy dependence on the volume fraction were constructed for the PMMA/SiO<sub>2</sub> model system. Only narrow window for achievement of individually dispersed NPs was found. It was found that the two observed cases of contact aggregates has different origin. The aggregates prepared from a solvent with the highest acid-base interaction enthalpy had the origin in a depletion attraction and thermodynamic character while the aggregates prepared

from a solvent with the lowest acid-base interaction enthalpy were formed due to an insufficient solvation of NPs by the solvent and had kinetic character.

Higher molecular weight and change of tacticity improved the dispersion state due to better steric stabilization<sup>93</sup> of longer chains and stronger adsorption of iso form of PMMA onto silica surface<sup>94, 95</sup>. Influence of NP-polymer and NP-NP interactions on final dispersion state was investigated on PNCs with various composition. Influence of various NPs was investigated in PNC with PMMA matrix. It was found that the dispersion state of NPs worsened in the order SiO<sub>2</sub>, AZO, and Fe<sub>2</sub>O<sub>3</sub> due to the increase of NP-NP interaction strength and decrease of NP-polymer interaction strength. Attractive NP-polymer interactions were mediated by acid-base interactions between acidic NP surface groups and basic PMMA functional groups. Therefore strength of NP-polymer interactions decreased with the strengthening acidic character of NPs. These results suggest that the NP-polymer interaction strength decreases in the order PMMA, PC, and PS due to the weakening of the polymer's basic character.

Precise NP spatial organization control brought unique opportunity to study the influence of PNC nanostructure on the relaxational and mechanical properties independently of the system composition – NP-polymer interaction strength. Systems with individually dispersed NPs enhanced the investigated properties the most followed by systems with chain bound clusters and systems with contact aggregates influenced the properties the least with some exceptions discussed later. Structure-independent correlation between glass transition temperature, reptation time, elastic modulus of PNCs and effective surface area was found. It was found that NPs significantly influence chain behavior in plateau region increasing number of entanglements per one chain and therefore act as entanglement attractors. The existing volume replacement continuum mechanics models<sup>72-74, 83-85</sup> for the composition dependence of the elastic and plateau modulus were not able to describe the dependence of relative modulus on the NP volume fraction. It is a clear evidence for adding another segment scale reinforcing mechanism into consideration. The results support immobilization concept, where adsorbed layer of polymer segments onto NP surface and a surrounding frustrated layer of polymer chains are assumed. Adsorption of polymer segments onto particle surface increased their hydrodynamic size that influenced the viscosity of PNCs. Adsorption coefficient was found to be the highest in PNCs with individually dispersed NPs and the lowest in PNCs with contact aggregates due to the effective surface area. PNCs with chain bound clusters had the highest particle interaction coefficient due to strong adsorbed chains mediated interactions of particles in closely packed clusters. Although PNCs with individually dispersed NPs increased yield stress the most in ductile flow controlled regime, PNCs with chain bound clusters had broadened the macroscopically ductile response to lower temperatures and over larger range of strain rates due to their hierarchical nature. Structure-related differences were found in long term mechanical properties. In contrast with another NP organizations, PNCs with individually dispersed NPs significantly improved time to failure compared to neat PMMA matrix.

Greater enhancement of reptation time and plateau modulus was determined for PMMA/SiO<sub>2</sub> PNCs with 500 kg/mol compared to 100 kg/mol matrix. Pronounced NP influence on relaxation properties of 500 kg/mol PNCs in terminal zone was probably caused by stronger adsorption of isotactic PMMA chains<sup>94, 95</sup> contained in greater amount in 500 kg/mol PMMA matrix. Also, larger frustrated layer is expected due to more preferable interparticle distance to polymer coil ratio. Therefore, more entanglements were induced by NPs and chain reptation was significantly slowed down because more chains had to pass through more and larger areas with affected dynamics. Minor influence of molecular weight and tacticity on stiffness was found while pronounced increase of yield stress was found for PNCs with 500 kg/mol

PMMA. It suggest stronger influence of the molecular weight and tacticity on the processes operating at longer time scale.

The greatest enhancement of properties was found for PMMA/SiO<sub>2</sub> system, where moderate-strong interaction are expected due to polar interactions and possible hydrogen bonding. PMMA acts as Lewis base due to its ester side groups. Silica, on the other hand, acts as Lewis acid due to silanol groups onto its surface. The properties were less influenced in the case of AZO NPs due to less acidic character of their surface. Only weak dipole–dipole interactions are expected in PS/SiO<sub>2</sub> PNCs in contrast with PMMA/SiO<sub>2</sub> PNCs, therefore only small influence on final properties was found in PS based PNCs. Properties of PC/SiO<sub>2</sub> PNCs were less enhanced than PMMA/SiO<sub>2</sub> PNCs due to weaker NP–polymer interaction strength.

Different influence of NPs on  $\alpha$  and  $\beta$  processes of yielding was found. The more local  $\beta$  process was almost unchanged. Increase of activation volume and energy of the cooperative  $\alpha$  process was found. It means that NPs affect preferably or in greater amount the chain dynamic at longer time and length scales. It led to a conclusion that frustrated layer between the immobilized segments and bulk chains has a greater impact on the large strain deformation behavior than surface immobilized layer. Polymer–NP interactions had stronger effect on  $\alpha$  process involving the entire backbone compared to  $\beta$  process presumably involving only few segments.

Correlation between relaxational and mechanical properties of PNCs was investigated. It was found that the strain rate dependence of neat PMMA matrix and PNCs converges into a single curve when reduced to the distance from the glass transition temperature. PNC samples were further from its glass transition, occupying a different location in energy landscape, than the neat PMMA matrix when measured at the same temperature. NPs significantly alter packing and dynamics of surrounding chains from the bulk state. A correlation of glass transition temperature and yield stress enhancement showed that the dynamics these processes operate at the same length and time scale. Strain hardening modulus did not correlate with glass transition. It means that dynamics at strain hardening regime is not similar with the local segmental dynamics. Strain hardening modulus was reduced to the number of entanglements per one chain. The PNC and the matrix data converged into a single curve. NPs act as entanglements attractors altering polymer dynamics in the plateau region. The results suggest that the dynamics responsible for the strain hardening response lies in the same time and length scale as the dynamics in the plateau region.

## 5. References

1. U. G. K. Wegst, H. Bai, E. Saiz, A. P. Tomsia and R. O. Ritchie, *Nature Materials*, 2015, **14**, 23-36.
2. Z. Nie, A. Petukhova and E. Kumacheva, *Nature Nanotechnology*, 2010, **5**, 15-25.
3. H. D. Espinosa, J. E. Rim, F. Barthelat and M. J. Buehler, *Progress in Materials Science*, 2009, **54**, 1059-1100.
4. J. Wang, Q. Cheng and Z. Tang, *Chemical Society Reviews*, 2012, **41**, 1111-1129.
5. H. B. Yao, H. Y. Fang, X. H. Wang and S. H. Yu, *Chemical Society Reviews*, 2011, **40**, 3764-3785.
6. M. A. Meyers, P. Y. Chen, M. I. Lopez, Y. Seki and A. Y. M. Lin, *Journal of the Mechanical Behavior of Biomedical Materials*, 2011, **4**, 626-657.
7. P. Y. Chen, A. Y. M. Lin, Y. S. Lin, Y. Seki, A. G. Stokes, J. Peyras, E. A. Olevsky, M. A. Meyers and J. McKittrick, *Journal of the Mechanical Behavior of Biomedical Materials*, 2008, **1**, 208-226.
8. J. Jancar, J. F. Douglas, F. W. Starr, S. K. Kumar, P. Cassagnau, A. J. Lesser, S. S. Sternstein and M. J. Buehler, *Polymer*, 2010, **51**, 3321-3343.
9. A. Hashemi, N. Jouault, G. A. Williams, D. Zhao, K. J. Cheng, J. W. Kysar, Z. Guan and S. K. Kumart, *Nano Letters*, 2015, **15**, 5465-5471.
10. J. Jordan, K. I. Jacob, R. Tannenbaum, M. A. Sharaf and I. Jasiuk, *Materials Science and Engineering a-Structural Materials Properties Microstructure and Processing*, 2005, **393**, 1-11.
11. M. E. Mackay, A. Tuteja, P. M. Duxbury, C. J. Hawker, B. Van Horn, Z. B. Guan, G. H. Chen and R. S. Krishnan, *Science*, 2006, **311**, 1740-1743.
12. N. Jouault, P. Vallat, F. Dalmas, S. Said, J. Jestin and F. Boue, *Macromolecules*, 2009, **42**, 2031-2040.
13. N. Jouault, F. Dalmas, F. Boue and J. Jestin, *Polymer*, 2012, **53**, 761-775.
14. C. Chevigny, N. Jouault, F. Dalmas, F. Boue and J. Jestin, *Journal of Polymer Science Part B-Polymer Physics*, 2011, **49**, 781-791.
15. N. Jouault, D. Zhao and S. K. Kumar, *Macromolecules*, 2014, **47**, 5246-5255.
16. D. Zhao, D. Schneider, G. Fytas and S. K. Kumar, *Acs Nano*, 2014, **8**, 8163-8173.
17. S. E. Harton, S. K. Kumar, H. Yang, T. Koga, K. Hicks, E. Lee, J. Mijovic, M. Liu, R. S. Vallery and D. W. Gidley, *Macromolecules*, 2010, **43**, 3415-3421.
18. L. S. Schadler, S. K. Kumar, B. C. Benicewicz, S. L. Lewis and S. E. Harton, *Mrs Bulletin*, 2007, **32**, 335-340.
19. S. Y. Kim and C. F. Zukoski, *Langmuir*, 2011, **27**, 10455-10463.
20. S. Y. Kim and C. F. Zukoski, *Langmuir*, 2011, **27**, 5211-5221.
21. S. Y. Kim and C. F. Zukoski, *Soft Matter*, 2012, **8**, 1801-1810.
22. S. Y. Kim, K. S. Schweizer and C. F. Zukoski, *Physical Review Letters*, 2011, **107**.
23. J. S. Meth, S. G. Zane, C. Chi, J. D. Londono, B. A. Wood, P. Cotts, M. Keating, W. Guise and S. Weigand, *Macromolecules*, 2011, **44**, 8301-8313.
24. D. W. Janes, J. F. Moll, S. E. Harton and C. J. Durning, *Macromolecules*, 2011, **44**, 4920-4927.
25. A. Bansal, H. C. Yang, C. Z. Li, K. W. Cho, B. C. Benicewicz, S. K. Kumar and L. S. Schadler, *Nature Materials*, 2005, **4**, 693-698.
26. L. M. Hamming, R. Qiao, P. B. Messersmith and L. C. Brinson, *Composites Science and Technology*, 2009, **69**, 1880-1886.
27. C. Hub, S. E. Harton, M. A. Hunt, R. Fink and H. Ade, *Journal of Polymer Science Part B-Polymer Physics*, 2007, **45**, 2270-2276.
28. C. Becker, H. Krug and H. Schmidt, San Francisco, Ca, 1996.

29. A. Bansal, H. Yang, C. Li, R. C. Benicewicz, S. K. Kumar and L. S. Schadler, *Journal of Polymer Science Part B-Polymer Physics*, 2006, **44**, 2944-2950.
30. S. Sen, Y. Xie, A. Bansal, H. Yang, K. Cho, L. S. Schadler and S. K. Kumar, *European Physical Journal-Special Topics*, 2007, **141**, 161-165.
31. P. D. Castrillo, D. Olmos, D. R. Amador and J. Gonzalez-Benito, *Journal of Colloid and Interface Science*, 2007, **308**, 318-324.
32. Y. H. Hu, C. Y. Chen and C. C. Wang, *Polymer Degradation and Stability*, 2004, **84**, 545-553.
33. J. L. H. Chau, C.-C. Hsieh, Y.-M. Lin and A.-K. Li, *Progress in Organic Coatings*, 2008, **62**, 436-439.
34. D. B. Stojanovic, L. Brajovic, A. Orlovic, D. Dramlic, V. Radmilovic, P. S. Uskokovic and R. Aleksic, *Progress in Organic Coatings*, 2013, **76**, 626-631.
35. A. Sargsyan, A. Tonoyan, S. Davtyan and C. Schick, *European Polymer Journal*, 2007, **43**, 3113-3127.
36. S. Etienne, C. Becker, D. Ruch, B. Grignard, G. Cartigny, C. Detrembleur, C. Calberg and R. Jerome, *Journal of Thermal Analysis and Calorimetry*, 2007, **87**, 101-104.
37. C. Triebel and H. Muenstede, *Polymer*, 2011, **52**, 1596-1602.
38. M. Hedayati, M. Salehi, R. Bagheri, M. Panjepour and A. Maghzian, *Powder Technology*, 2011, **207**, 296-303.
39. H. Weickmann, R. Delto, R. Thomann, R. Brenn, W. Doell and R. Muelhaupt, *Journal of Materials Science*, 2007, **42**, 87-92.
40. D. Cangialosi, V. M. Boucher, A. Alegria and J. Colmenero, *Polymer*, 2012, **53**, 1362-1372.
41. C. C. Neikirk, J. W. Chung and R. D. Priestley, *Rsc Advances*, 2013, **3**, 16686-16696.
42. D. Maillard, S. K. Kumar, B. Fragneaud, J. W. Kysar, A. Rungta, B. C. Benicewicz, H. Deng, L. C. Brinson and J. F. Douglas, *Nano Letters*, 2012, **12**, 3909-3914.
43. J. Kalfus and J. Jancar, *Journal of Polymer Science Part B-Polymer Physics*, 2007, **45**, 1380-1388.
44. J. Kalfus and J. Jancar, *Polymer*, 2007, **48**, 3935-3937.
45. J. Kalfus and J. Jancar, *Polymer Composites*, 2007, **28**, 365-371.
46. J. Kalfus and J. Jancar, *Polymer Composites*, 2007, **28**, 743-747.
47. D. R. Paul and L. M. Robeson, *Polymer*, 2008, **49**, 3187-3204.
48. P. Rittigstein and J. M. Torkelson, *Journal of Polymer Science Part B-Polymer Physics*, 2006, **44**, 2935-2943.
49. J. Moll and S. K. Kumar, *Macromolecules*, 2012, **45**, 1131-1135.
50. B. J. Ash, L. S. Schadler and R. W. Siegel, *Materials Letters*, 2002, **55**, 83-87.
51. J. Jancar, R. S. Hoy, A. J. Lesser, E. Jancarova and J. Zidek, *Macromolecules*, 2013, **46**, 9409-9426.
52. J. Jancar, R. S. Hoy, E. Jancarova and J. Zidek, *Polymer*, 2015, **63**, 196-207.
53. D. Zhao, V. Gimenez-Pinto, A. M. Jimenez, L. X. Zhao, J. Jestin, S. K. Kumar, B. Kuei, E. D. Gomez, A. S. Prasad, L. S. Schadler, M. M. Khani and B. C. Benicewicz, *Acs Central Science*, 2017, **3**, 751-758.
54. J. Khan, S. E. Harton, P. Akcora, B. C. Benicewicz and S. K. Kumar, *Macromolecules*, 2009, **42**, 5741-5744.
55. J. Jancar and K. Fiore, *Polymer*, 2011, **52**, 5851-5857.
56. Y. Zhou, J. L. He, J. Hu and B. Dang, *Journal of Applied Polymer Science*, 2016, **133**.
57. F. W. Starr, J. F. Douglas and S. C. Glotzer, *Journal of Chemical Physics*, 2003, **119**, 1777-1788.
58. J. Zidek, J. Kucera and J. Jancar, *Cmc-Computers Materials & Continua*, 2010, **16**, 51-73.

59. J. Zidek, J. Kucera and J. Jancar, *Cmc-Computers Materials & Continua*, 2011, **24**, 183-208.
60. M. J. Marmo, M. A. Mostafa, H. Jinnai, F. M. Fowkes and J. A. Manson, *Industrial & Engineering Chemistry Product Research and Development*, 1976, **15**, 206-211.
61. F. M. Fowkes and M. A. Mostafa, *Industrial & Engineering Chemistry Product Research and Development*, 1978, **17**, 3-7.
62. F. M. Fowkes, *Rubber Chemistry and Technology*, 1984, **57**, 328-343.
63. D. L. Allara, F. M. Fowkes, J. Noolandi, G. W. Rubloff and M. V. Tirrell, *Materials Science and Engineering*, 1986, **83**, 213-226.
64. F. M. Fowkes, *Journal of Adhesion Science and Technology*, 1990, **4**, 669-691.
65. R. S. Drago, G. C. Vogel and T. E. Needham, *Journal of the American Chemical Society*, 1971, **93**, 6014-&.
66. G. P. Vanderbeek, M. A. C. Stuart, G. J. Fleer and J. E. Hofman, *Macromolecules*, 1991, **24**, 6600-6611.
67. T. Hamieh, J. Toufaily and M. B. Fadlallah, *Advanced Powder Technology*, 2003, **14**, 547-558.
68. R. A. Riggleman, G. Toepperwein, G. J. Papakonstantopoulos, J.-L. Barrat and J. J. de Pablo, *Journal of Chemical Physics*, 2009, **130**.
69. G. J. Schneider, *Current Opinion in Chemical Engineering*, 2017, **16**, 65-77.
70. J. Berriot, H. Montes, F. Lequeux, D. Long and P. Sotta, *Macromolecules*, 2002, **35**, 9756-9762.
71. A. Mujtaba, M. Keller, S. Ilisch, H. J. Radusch, M. Beiner, T. Thurn-Albrecht and K. Saalwachter, *Acs Macro Letters*, 2014, **3**, 481-485.
72. E. Guth and O. Gold, *Phys. Rev.*, 1938, **53**, 322.
73. H. M. Smallwood, *J. Appl. Phys.*, 1944, **15**, 758.
74. E. Guth, *Appl. Phys.*, 1945, **16**, 20.
75. J. Jancar and L. Recman, *Polymer*, 2010, **51**, 3826-3828.
76. S. Merabia, P. Sotta and D. R. Long, *Macromolecules*, 2008, **41**, 8252-8266.
77. P. Sotta, P. A. Albouy, M. Abou Taha, D. R. Long, P. Grau, C. Fayolle and A. Papon, *Macromolecules*, 2017, **50**, 6314-6322.
78. B. J. Anderson and C. F. Zukoski, *Macromolecules*, 2008, **41**, 9326-9334.
79. B. J. Anderson and C. F. Zukoski, *Macromolecules*, 2009, **42**, 8370-8384.
80. B. J. Anderson and C. F. Zukoski, *Langmuir*, 2010, **26**, 8709-8720.
81. S. Mueller, E. W. Llewellyn and H. M. Mader, *Proceedings of the Royal Society a-Mathematical Physical and Engineering Sciences*, 2010, **466**, 1201-1228.
82. P. G. Debenedetti and F. H. Stillinger, *Nature*, 2001, **410**, 259-267.
83. E. H. Kerner, *Proceedings of the Physical Society*, 1956, **69B**, 808.
84. L. E. Nielsen, *Journal of Applied Physics*, 1970, **41**, 4626-&.
85. L. E. Nielsen and R. F. Landel, *Mechanical properties of polymers and composites*, New York, 1994.
86. A. Dorigato, M. Sebastiani, A. Pegoretti and L. Fambri, *Journal of Polymers and the Environment*, 2012, **20**, 713-725.
87. B. Pukanszky, *Composites*, 1990, **21**, 255-262.
88. L. Nicolais and M. Narkis, *Polymer Engineering and Science*, 1971, **11**, 194-&.
89. S. C. Bellemare, M. N. Bureau, J. Denault and J. I. Dickson, *Polymer Composites*, 2004, **25**, 433-441.
90. M. H. R. Jen, Y. C. Tseng and C. H. Wu, *Composites Science and Technology*, 2005, **65**, 775-779.
91. R. Ormsby, T. McNally, P. O'Hare, G. Burke, C. Mitchell and N. Dunne, *Acta Biomaterialia*, 2012, **8**, 1201-1212.

92. T. Takeda, Y. Shindo, Z. J. Wei, Y. Kurohuma and F. Narita, *Journal of Composite Materials*, 2015, **49**, 457-463.
93. J. B. Hooper and K. S. Schweizer, *Macromolecules*, 2005, **38**, 8858-8869.
94. T. Hamieh and J. Schultz, *Journal of Chromatography A*, 2002, **969**, 27-36.
95. T. Hamieh, M. B. Fadlallah and J. Schultz, *Journal of Chromatography A*, 2002, **969**, 37-47.

## 6. Author's CV

### PERSONAL INFORMATION

František Ondreáš  
[frantisek.ondreas@ceitec.vutbr.cz](mailto:frantisek.ondreas@ceitec.vutbr.cz)

### WORK EXPERIENCE

- 03/2013 – Present     *Material Science Technician – Ph.D. student*  
Central European Institute of Technology, Brno University of Technology,  
Advanced Polymers and Composites  
- research on polymer nanocomposites and writing of scientific papers  
- preparation and characterization of polymer nanocomposites by structural,  
thermal, and mechanical testing
- 03/2017 – 02/2018     *Material Development Engineer*  
Unipetrol RPA, s.r.o. – Polymer Institute Brno, odštepny závod  
- research on degradation and stabilization of polymers  
- product development and technical support of polymer stabilization systems  
- accelerated weathering testing
- 09/2016 – 12/2016     *Internship*  
Polymer Technology Group, Department of Mechanical Engineering, Eindhoven  
University of Technology  
- research on mechanical properties of polymer nanocomposites  
- mechanical testing of polymers and their nanocomposites
- 02/2012 – 12/2012     *Material Science Technician*  
Brno University of Technology, Faculty of Chemistry  
- research on plasma polymerized thin films  
- preparing thin films by PE-CVD and their structural characterization by infrared  
spectroscopy and spectroscopic ellipsometry
- 10/2011 – 12/2011     *Material Science Technician*  
Brno University of Technology, Faculty of Chemistry  
- preparation thin films by PE-CVD nad their structural characterization by  
infrared spectroscopy and spectroscopic ellipsometry

### EDUCATION

- 09/2014 – 12/2018     *Ph.D. degree*  
Central European Institute of Technology, Brno University of Technology  
Advanced materials
- 06/2012 – 06/2014     *Master degree with honors*  
Brno University of Technology, Faculty of Chemistry  
Chemistry, technology and properties of materials

08/2009 – 06/2012 *Bachelor degree with honors*  
Brno University of Technology, Faculty of Chemistry  
Chemistry, technology and properties of materials

#### ADDITIONAL INFORMATIONS

- Honors and awards    Josef Hlavka Award 2015 for talented students  
Employee of the year 2017 Unipetrol RPA, s.r.o. – Polymer Institute Brno
- Publications        Ondreas, F.; Lepcio, P.; Zarybnicka, K.; Zboncak, M.; Govaert, L.E.; Jancar, J. The effect of the nanoparticle organization on the relaxation and mechanical properties of polymer nanocomposites. Submitted to *Macromolecules* **2018**.  
Ondreas, F.; Jancar, J. Temperature, Frequency, And Small Static Stress Dependence Of The Molecular Mobility In Deformed Amorphous Polymers Near Their Glass Transition. *Macromolecules* **2015**, *48*, 4702-4716.  
Lepcio, P.; Ondreas, F.; Zarybnicka, K.; Zboncak, M.; Caha, O.; Jancar, J. Bulk polymer nanocomposites with preparation protocol governed nanostructure: the origin and properties of aggregates and polymer bound clusters. *Soft Matter* **2018**, *14* (11), 2094-2103.  
Cech, V.; Knob, A.; Hosein, H. -A.; Babik, A.; Lepcio, P.; Ondreas, F.; Drzal, L. T. Enhanced Interfacial Adhesion Of Glass Fibers By Tetravinylsilane Plasma Modification. *Composites Part A: Applied Science and Manufacturing* **2014**, *58*, 84-89.  
Lepcio, P.; Ondreas, F.; Jancar, J. Rheological Behavior Of Polystyrene-Based Nanocomposite Suspensions Under Laos. *Materials Science Forum* **2016**, *851*, 215-220.  
Zboncak, M.; Ondreas, F.; Jancar, J. Force-Assembled Fe<sub>3</sub>O<sub>4</sub> Particle Chains In Polyurethane Matrix. *Materials Science Forum* **2016**, *851*, 221-225.
- Projects              TA62804000 – Recycling of waste polycarbonates and development of advanced thermoplastic blends with polycarbonate part usable in primary production application  
STI-J-17-4204 – Mechanical properties of polymer nanocomposites with controlled structure  
STI-J-16-3650 – Governing of nanoparticle self-assembly in polymer liquids and influence of formed nanostructure on thermomechanical behavior of final nanocomposites  
STI-J-17-4295 – Magnetic field directed self-assembly as rout for bottom-up build-up approach inspired by nature  
STI-J-15-2856 – Influence of kinetic and thermodynamic preparation conditions on dispersion states of polymer nanocomposites and their thermomechanical properties
- Skills                 - experience in teamwork gained during solving research projects  
- creativity in searching for new theoretical and experimental approaches and solving problems in material science

## 7. Abstract

This thesis is focused on a fundamental investigation of nanoparticle self-assembly in polymer liquids and on properties of the prepared polymer nanocomposites with controlled nanoparticle dispersion. Despite recent progress in understanding polymer nanocomposites, there are still unfilled gaps in the fundamental knowledge of relaxation phenomena and mechanical properties of various nanostructures that would provide key information for designing hierarchical or multidomain nanocomposites processable by additive manufacturing technologies. The emphasis was put on the investigation of the preparation protocol influence on the final dispersion state, preparation of various nanostructures – individually dispersed NPs, chain bound clusters, and contact aggregates at a constant composition, and determination of their relaxation and mechanical properties. Moreover, nanoparticles were utilized as “probes” in polymer matrix that affect the segmental ordering and the relaxation dynamics of polymer chains. This approach can help to derive the relationship between the nano scale segmental dynamics and macro scale mechanical properties of polymer glasses. It is a challenging fundamental scientific problem with an extreme technological importance. Non-grafted ceramic nanoparticles and polymer glasses were used to avoid the focus to deflect from the study of the nanoparticle–polymer interaction influence towards the influence of the graft–polymer interaction or the altered crystalline structure. A thorough investigation was performed for the PMMA/SiO<sub>2</sub> model system and subsequently broadened to systems with different matrices (PC and PS) and nanoparticles (ZnO<sub>2</sub> and Fe<sub>2</sub>O<sub>3</sub>) in order to generalize the obtained results. Nanostructure, volume fraction, and composition dependences of relaxation – glass transition temperature, reptation time, plateau modulus, number of entanglements, and mechanical properties – yield stress, yield drop, elastic modulus, strain hardening modulus, and creep response were determined. Achieved results were interpreted by means of the recent models. The determined relaxational and mechanical properties were connected to provide information about the molecular processes responsible for the mechanical response of the polymer nanocomposites.